11. R.C.R. Yahiaoui, N. Chevalier, M. Jouvet, and M. Lalande, Metamaterial-based highly directive antenna: Application in a monochromatic wave radar for a contactless measurement of the breathing activity, Prog Electromagn Res C 44 (2013), 185–195.
12. K.R. Carver and J. Mink, Microstrip antenna technology, IEEE Trans Antennas Propag 29 (1981), 2–24.
13. H. Majid and M. Rahim, Parametric studies on left-handed metamaterial consist of modified split-ring resonator and capacitance loaded strip, Appl Phys A 103 (2011), 607–610.

MIMO MULTIBAND ANTENNA SYSTEM WITH NONRESONANT ELEMENTS

Aurora Andújar[1] and Jaume Anguera[1,2]
[1] Technology and Intellectual Property Rights Department, Fractus, C/Alcalde Barnils n°64, 08174 Barcelona, Spain
[2] Electronics and Telecommunications Department, Universitat Ramon Llull, 08022 Barcelona, Spain

Received 5 June 2014

ABSTRACT: *Multi-input multi-output (MIMO) technology will enable high-data rates in wireless devices to allow speech and video calls to streaming media and web browsing all over a common platform. MIMO technology needs M antennas both in transmission and reception. As the space in a wireless device is limited, including M antennas is a challenge. To face such challenge, a MIMO antenna system is proposed which comprises two small nonresonant elements operating in the frequency region 824–960 MHz and two identical elements operating at 1710–2170 MHz. The size of each of the nonresonant elements is only 5 × 5 × 5 mm^3. The proposed MIMO system is analyzed in terms of bandwidth, efficiency, correlation, and multiplexing efficiency. MIMO capacity is measured in a reverberation chamber considering a free-space Rayleigh scenario and also including the effect of a phantom head and hand. The results reveal that the proposed MIMO system provides capacity close to the ideal bound while having a small size and able to operate at several 2G, 3G, and 4G long term evolution standards.* © 2015 Wiley Periodicals, Inc. Microwave Opt Technol Lett 57:183–190, 2015; View this article online at wileyonlinelibrary.com. DOI 10.1002/mop.28810

Key words: *handset antennas; low-volume antenna; multiband; nonresonant antennas; MIMO; correlation; isolation; multiplexing efficiency; capacity; reverberation chamber*

1. INTRODUCTION

The rapid growth of mobile communications has fostered the appearance of new communication standards capable of providing high data rates. This is the case of long term evolution (LTE), which consolidates as the 4G solution that will naturally follow today's 3G UMTS Technology [1].

The challenges of designing multiband and small handset antennas have been significantly exacerbated with the appearance of the MIMO technology. MIMO systems require the integration of multiple antennas in transmission and reception to provide high speed data rates. To preserve the benefits of the technology, these multiple antennas operating in the same number of frequency bands, must be sufficiently uncorrelated and isolated.

The previous solutions disclosed in the literature for providing a wireless handheld or portable device integrating the MIMO technology are usually based on antenna elements with a size comparable to the wavelength of operation [2–5]. These MIMO solutions usually operate at a frequency located in a high frequency region (∼2 GHz) where the operating wavelength is small enough to allow the integration of several antenna elements with dimensions close to a quarter of a wavelength. Therefore, these proposals are still antenna-based solutions as the contribution to the radiation is predominantly provided by the antenna. This limitation prevents the possibility of arranging large number of antenna elements, as on one hand, the available space in the wireless handheld or portable device is limited, and conversely, undesired coupling effects appear due to the proximity between the antenna elements, more significantly when operation in low frequency regions, such as those allocating the LTE700 communication standard, is demanded.

Other attempts are focused on antenna elements not requiring a complex geometry while still providing some degree of miniaturization using an antenna element that is not resonant in the frequency regions of operation of the wireless handheld or portable device [6–10]. The solution presented in [6] is based on this concept and provides operation in DVB-H communication standard, which is located in a low frequency region (470–862 MHz). Although some miniaturization is achieved, such a solution is not enough to provide low correlation and low coupling or high isolation between these antenna elements. Owing to such limitations, while the MIMO performance of the former solution may be sufficient for reception of electromagnetic wave signals, the antenna elements still could not provide an adequate MIMO behavior (e.g., in terms of input return losses or gain) for a cellular communication standard requiring also the transmission of a significant amount of power in the form of electromagnetic wave signals. At the same time, those solutions providing suitable transmission and reception of electromagnetic wave signals, such as those described in [7–9], are limited to single band operation.

Many are the efforts in the literature focused on reducing mutual coupling and correlation. The most common techniques rely on spacing the multiple antennas a sufficient distance, preferably larger than 0.5λ, as for achieving high port-to-port isolation [11,12]. Although this mechanism becomes suitable for high frequency operation (∼2 GHz), the limited dimensions of current handset platforms make it unsuitable for antennas operating at low frequency regions (∼0.9 GHz). Other techniques reduce the correlation between antenna elements by providing significantly different radiation patterns or polarizations [13]. The antenna elements operate at the 2.6 GHz LTE/WiFi band (2.5–2.7 GHz) and are oriented orthogonally to each other. Nevertheless, at low frequency regions below 1 GHz where the ground plane behaves as the main radiator, the required orthogonal feature is considerably difficult to achieve.

Balanced antennas appear as an alternative solution for reducing mutual coupling [14,15]. They prevent the appearance of currents in the ground plane, which leads to high isolation values between antenna ports. However, the main inconvenience of these solutions is again found in frequency regions below 1 GHz.

Other studies deal with the reduction of the mutual coupling and the correlation values by providing modifications in the ground plane, such as adding quarter wavelength slots [16,17] or quarter-wavelength stubs [18–20]. Alternatively, several attempts address this challenge by integrating hybrid couplers [21–24], decoupling networks [25,26], or neutralization lines [27–29] inside the handset platform to enhance the correlation and isolation. Finally, other attempts suggest the use of dielectric antennas due to their capabilities of near-field confinement [30]. Nevertheless, some cost, complexity and losses problems arise when regarding this kind of antenna elements.

The article is divided as follows: a basic description of the metric to characterize a MIMO antenna system is briefly

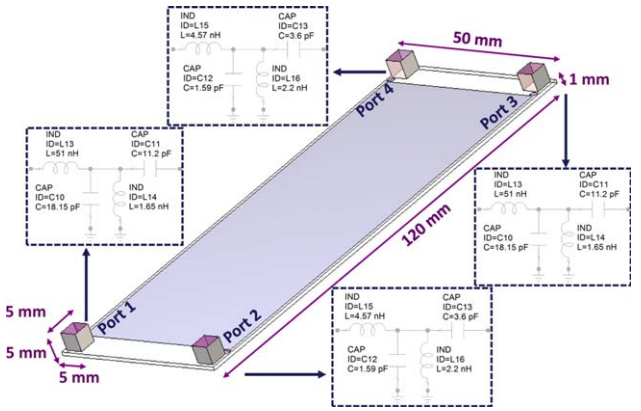

Figure 1 Geometry of the proposed multiband MIMO system comprising four nonresonant elements placed at the corners of a ground plane (120 × 50 mm^2). The ground plane is etched over a 1 mm thick FR4 piece ($\varepsilon_r = 4.15$, tanδ = 0.013). The matching network connected to each port contains a series inductor, a broadband matching network, and a series capacitor as a fine tuning stage. [Color figure can be viewed in the online issue, which is available at wileyonlinelibrary.com]

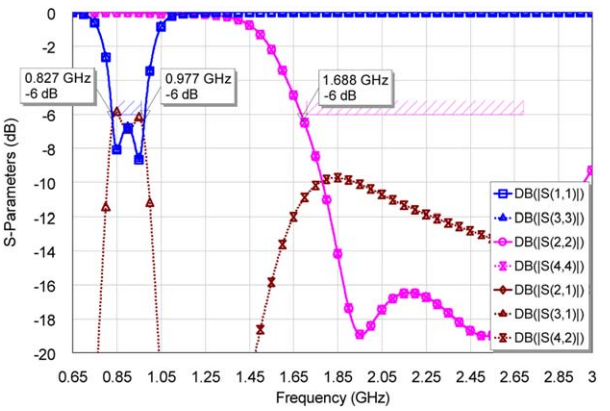

Figure 2 *S*-parameters for the scheme shown in Figure 1. [Color figure can be viewed in the online issue, which is available at wileyonlinelibrary.com]

explained in Section 2. Simulated results of a multiband MIMO system are gathered in Section 3. Measurements results showing reflection coefficient, isolation, envelope correlation, multiplexing efficiency are presented in Section 4. Section 5 discusses the results of the measured MIMO capacity in a reverberation chamber. Finally, conclusions are derived in Section 6.

2. THE RADIATING SYSTEM

MIMO antennas must be as uncorrelated as possible to preserve independent propagation paths. In this sense, they should be as uncoupled as possible because mutual coupling between antenna elements considerably degrades correlation as well as decreases the radiated power. Ideally, the correlation between antennas should be zero, although values smaller than 0.5 are also acceptable. In this article, correlation coefficient is derived from far-field radiation patterns regarding an isotropic propagation environment (1).

$$\rho_e = \frac{\left|\iint_{4\pi}\left[\vec{F}_1(\theta,\varphi)\cdot\vec{F}_2^{*}(\theta,\varphi)d\Omega\right]\right|^2}{\iint_{4\pi}|\vec{F}_1(\theta,\varphi)|^2 d\Omega\cdot\iint_{4\pi}|\vec{F}_2(\theta,\varphi)|^2 d\Omega} \quad (1)$$

Furthermore, as two antennas of a MIMO system can present a low correlation but poor efficiency, a new parameter that takes into account both effects has been proposed in the literature as multiplexing efficiency (η_{MUX}) [31]. η_{MUX} is defined as the difference in dBs of the signal to noise ratio (SNR) of an ideal MIMO system and the required SNR of the MIMO system under test to achieve the same channel capacity. It can be calculated from the antenna efficiencies (η_1, η_2) and envelope correlation ρ_e:

$$\eta_{MUX} = \sqrt{\eta_1\cdot\eta_2\cdot(1-\rho_e)} \quad (2)$$

where η_1, η_2 take into account both radiation efficiency and mismatching.

3. MULTI-BAND MIMO DESIGN: SIMULATED RESULTS

The proposal has been simulated by means of the software IE3D based on the method of moments. First of all, the behavior of a MIMO system based on nonresonant elements is analyzed [32–36]. The nonresonant elements are placed at the respective four corners of the ground plane, as being the preferable location of capacitive nonresonant elements. Those in charge of the same frequency region are placed in diagonally opposite corners to reduce mutual coupling (Fig. 1). It should be note that [37] shows an identical radiating structure however with a completely different architecture. In particular, in the present proposal, those nonresonant elements in charge of the same frequency region are used for MIMO, that is, it is a two port solution (the same applies for the other frequency region). However, in [37] it is not a MIMO solution. In particular, those nonresonant elements in charge of a frequency region are connected so as to provide a robust system to hand-loading. Therefore, there is no MIMO as for a frequency region there is only one port.

The simulated results demonstrate that the two nonresonant elements associated to the low frequency region (port 1 and port 3) are able of operating the standards GSM850 and GSM900, whereas those intended for the high frequency region offer a large impedance bandwidth (from 1.69 GHz up to beyond 3 GHz) (SWR ≤ 3), hence covering six additional communication standards, GSM1800, GSM1900, UMTS, LTE2100, LTE2300, and

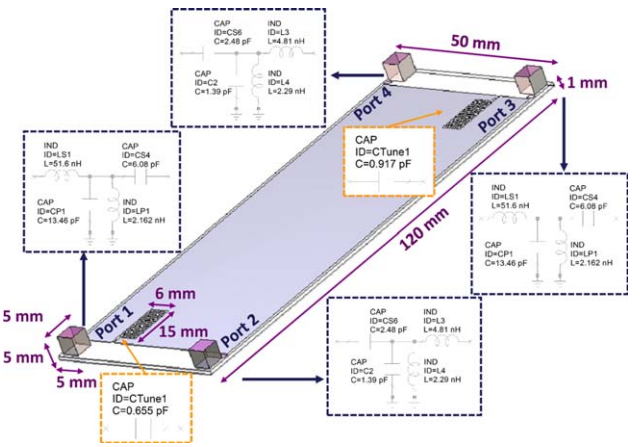

Figure 3 Geometry of the proposed multiband MIMO system comprising four nonresonant elements and two slots inspired in the Hilbert fractal. The ground plane is etched over a 1 mm thick FR4 piece ($\varepsilon_r = 4.15$, tan $\delta = 0.013$). [Color figure can be viewed in the online issue, which is available at wileyonlinelibrary.com]

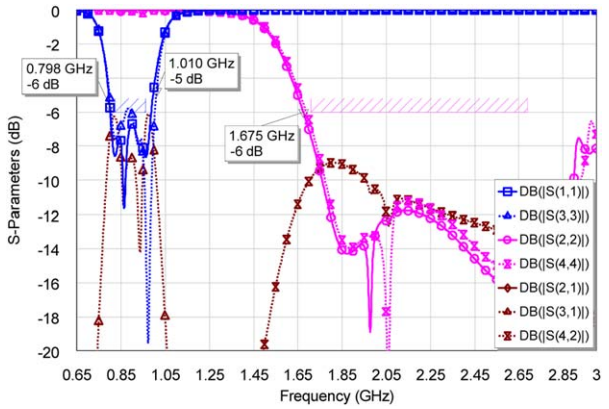

Figure 4 *S*-parameters for the multiband MIMO system of Figure 3. [Color figure can be viewed in the online issue, which is available at wileyonlinelibrary.com]

LTE2500 (port 2 and port 4). The transmission coefficient for the high frequency region remains below −10 dBs, whereas at the low frequency region it reaches peaks of −6 dBs (Fig. 2).

To reduce the coupling appearing between those nonresonant elements operating in the same frequency region, two slots inspired in the Hilbert fractal are etched in the respective shortest edges of the ground plane. In this case and with the aim of enhancing the

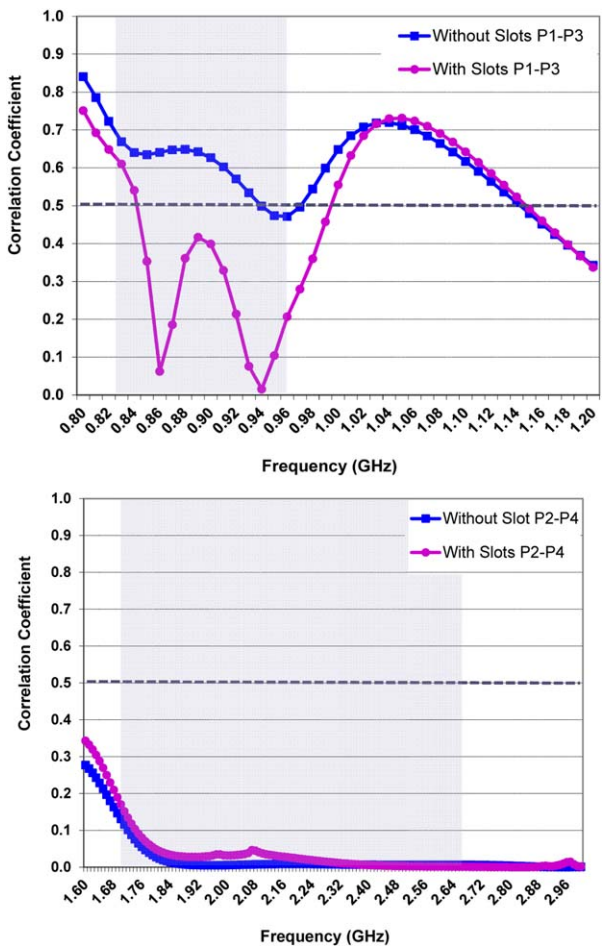

Figure 5 Correlation coefficient computed regarding radiation patterns (1) for the low and high frequency region, respectively. [Color figure can be viewed in the online issue, which is available at wileyonlinelibrary.com]

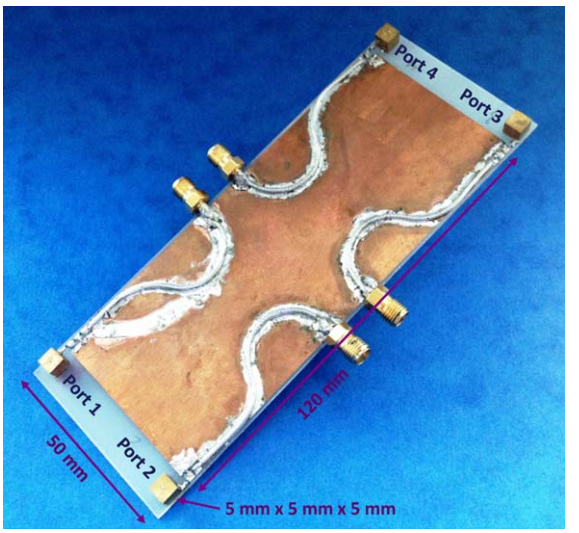

Figure 6 Geometry of the proposed multiband MIMO system comprising four nonresonant elements. The ground plane is etched over a 1 mm thick FR4 piece ($\varepsilon_r = 4.15$, tan $\delta = 0.013$). [Color figure can be viewed in the online issue, which is available at wileyonlinelibrary.com]

bandwidth where the transmission coefficient remains below a certain value, two slots are proposed, each one tuned at a particular frequency of the low frequency region (Fig. 3).

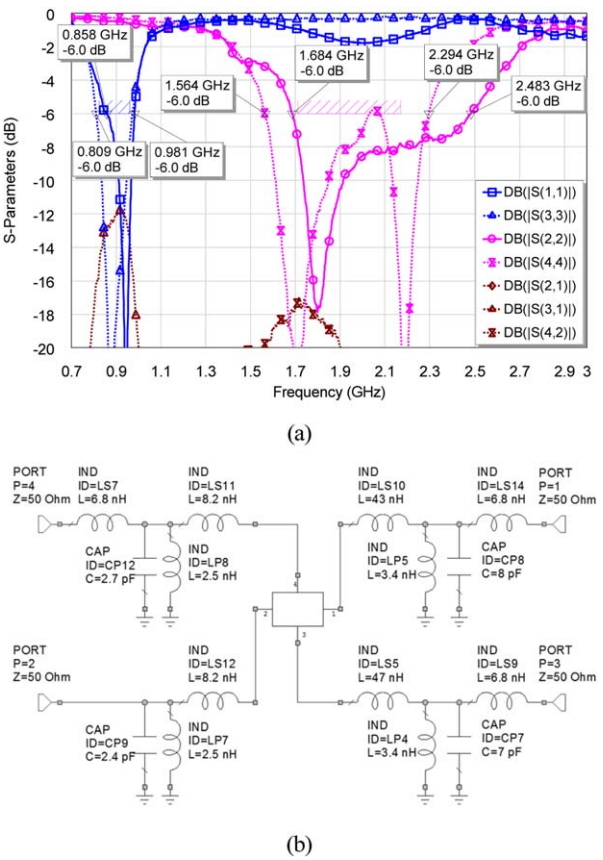

Figure 7 a) *S*-parameters. Port 1 and port 3 relate to the nonresonant elements intended for the low frequency region whereas port 2 and port 4 refers to those in charge of the high frequency range; b) schematic representation of the implemented matching networks containing the commercial values of the reactive elements (Murata 0402). [Color figure can be viewed in the online issue, which is available at wileyonlinelibrary.com]

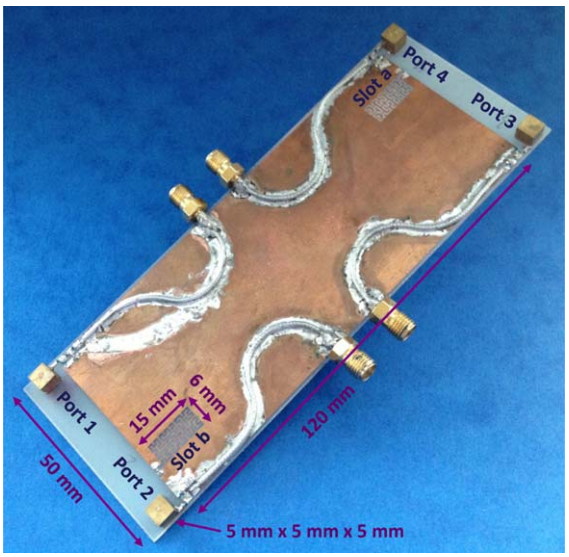

Figure 8 Geometry of the proposed multiband MIMO system comprising the four nonresonant elements and two slots inspired in the Hilbert geometry. The ground plane is etched over a 1 mm thick FR4 piece ($\varepsilon_r = 4.15$, tan $\delta = 0.013$). [Color figure can be viewed in the online issue, which is available at wileyonlinelibrary.com]

The Hilbert-based geometry has been selected as being a geometry able to pack long operating wavelengths into a reduced space [38,39].

In addition to the miniaturization capabilities provided by the own geometry, the dimensions of the proposed slots inspired in the Hilbert fractal are further minimized thanks to the addition of a reactive element, namely a capacitor placed close to the open edges of the Hilbert slot (Fig. 3).

The matching network topologies used in this case are equivalent to those needed in the case where the slots were not considered. Thus, port 1 and port 3 intended for the low frequency region require a series inductor, a broadband matching network, and a series capacitor as a fine tuning stage. The same topology applies to the high frequency region (port 2 and port 4). The impedance bandwidth is not altered by the integration of the slots and it continues offering operation in the low frequency region (824–960 MHz) and operation in the high frequency

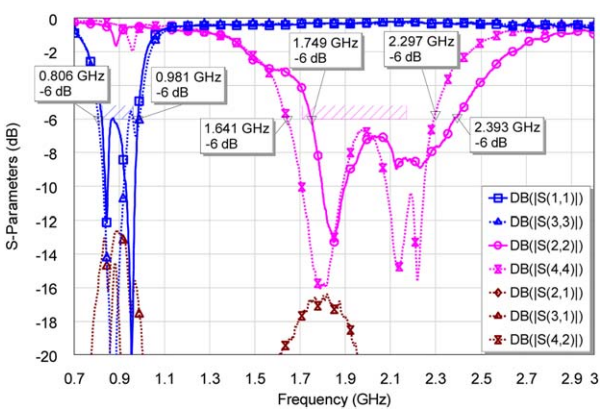

Figure 9 Measured *S*-parameters for the prototype of Figure 8. Port 1 and 3 refer to the nonresonant elements intended for the low frequency region, whereas port 2 and 4 relate to those in charge of the high frequency region. [Color figure can be viewed in the online issue, which is available at wileyonlinelibrary.com]

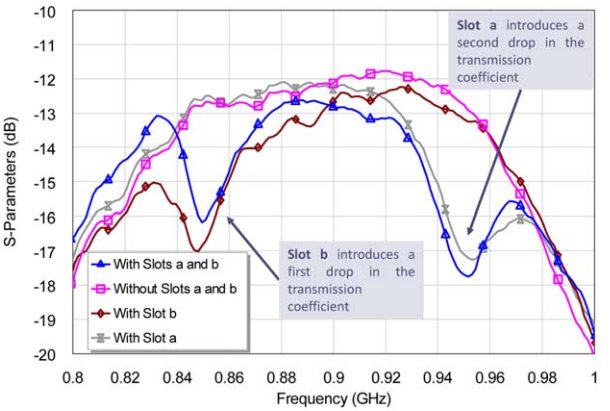

Figure 10 Effect of the Hilbert slots over the transmission coefficient. [Color figure can be viewed in the online issue, which is available at wileyonlinelibrary.com]

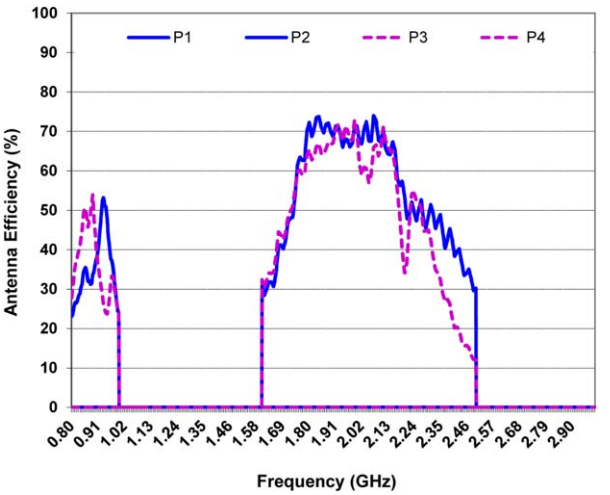

Figure 11 Antenna efficiency corresponding to the MIMO system illustrated in Figure 8. Port 1 and 3 refer to the nonresonant elements intended for the low frequency region, whereas port 2 and 4 relate to those in charge of the high frequency region. [Color figure can be viewed in the online issue, which is available at wileyonlinelibrary.com]

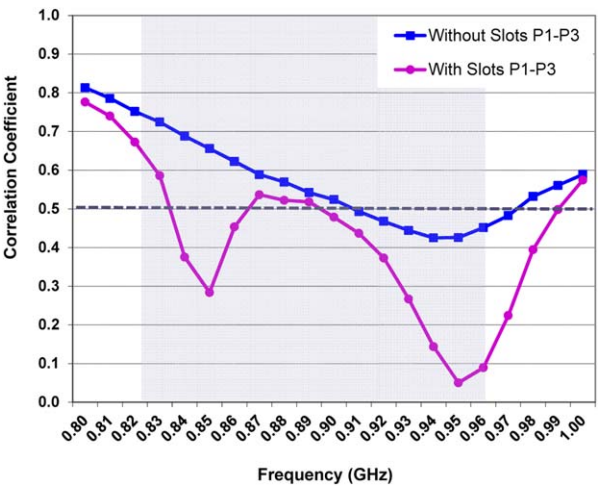

Figure 12 Correlation coefficient computed regarding the measured radiation patterns for the low frequency region. [Color figure can be viewed in the online issue, which is available at wileyonlinelibrary.com]

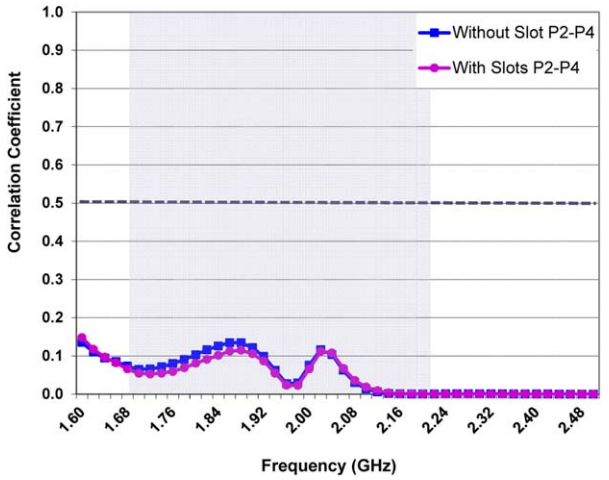

Figure 13 Correlation coefficient computed regarding the measured radiation patterns for the high frequency region. [Color figure can be viewed in the online issue, which is available at wileyonlinelibrary.com]

region (1710–2170 MHz). Moreover, they significantly contribute to minimize the transmission coefficient, more significantly at the low frequency region where the integration of the slots produces minimums around −12 and −14 dBs (Fig. 4).

Owing to the correlation, the proposal based on the integration of the two Hilbert-based slots in the ground plane significantly reduces correlation values with respect to the proposal that does not integrate the slots, when regarding the low frequency region (Fig. 5).

As discussed in the previous section, the correlation values for the high frequency region are below the required threshold of 0.5 for a large range of frequencies. At these high frequencies, the electrical distance is large enough as for guarantee low correlation coefficients even when having similar or equal radiation patterns, thus avoiding the need of including mechanisms to reduce isolation and correlation. Nevertheless, at the low frequency region, they are strongly required. In view of the results, the proposal becomes a feasible solution to reduce not only isolation (Fig. 4) but also to minimize correlation (Fig. 5) at these low frequencies. In addition, it provides the flexibility to tune the correlation nulls at the desired frequencies, because they can be easily adjusted through the series capacitor connected to the open edges of the Hilbert-based slots.

4. MULTI-BAND MIMO DESIGN: EXPERIMENTAL RESULTS

To validate the simulated results, two prototypes are built for measuring the MIMO performance. In this sense, four nonresonant elements have been placed in the respective four corners of a ground plane having typical dimensions of smartphone platforms (120 × 50 mm^2). The nonresonant elements are made of a solid piece of brass and the dimensions of each one are 5 × 5 × 5 mm^3 (Fig. 6). The measured *S*-parameters depict that the nonresonant elements intended for the low frequency region (port 1 and port 3) are able of operating the communication standards GSM850 and GSM900 and those in charge of the high frequency region attain a sufficient impedance bandwidth as for covering GSM1800, GSM1900, UMTS, and LTE2100 (a). The detailed view of the prototype illustrates how the proposed matching networks are connected at each port (b). The matching network topology illustrated in the simulated results (Fig. 3) is maintained in the prototyped solution. Accordingly, each port is connected to a series inductor and to a broadband matching network (b). In this case, the fine tuning stage is used for the low frequency region. The MIMO system under study presents a transmission coefficient that remains below −12 and −18 dBs, for the low and high frequency region, respectively (a). The measured antenna efficiencies values are, in average, around 38% and 65% for the low and high frequency region, respectively.

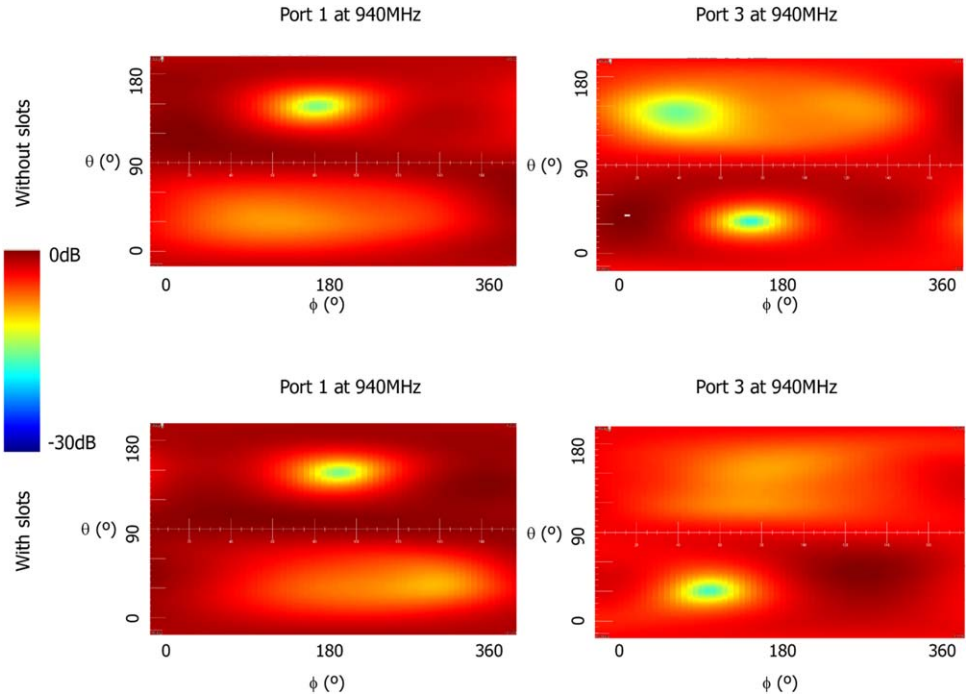

Figure 14 Comparison of the radiation patterns associated to each one of the ports of the low frequency region at a frequency where the correlation minimum appears regarding both configurations, with and without slots. [Color figure can be viewed in the online issue, which is available at wileyonlinelibrary.com]

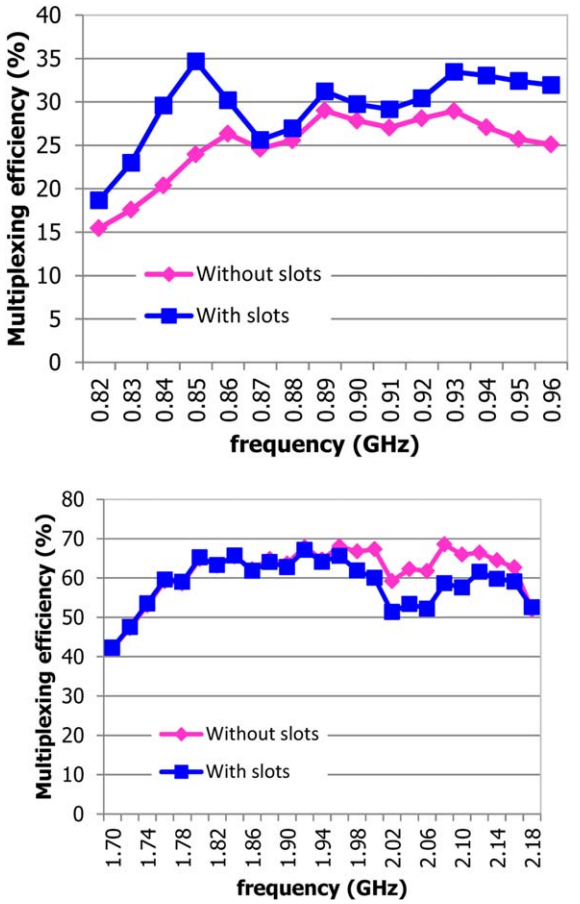

Figure 15 Multiplexing efficiency from the measured correlation and antenna efficiencies without and with the slots in the ground plane. [Color figure can be viewed in the online issue, which is available at wileyonlinelibrary.com]

To further improve the transmission coefficient as well as the correlation values in the low frequency range, two slots inspired in the Hilbert geometry are etched at the respective shortest edges of the ground plane (Fig. 8). As explained in the former section, a capacitor is connected to the open edge of each one of the slots with the aim of attaining further miniaturization.

As expected, the slots reduce the most critical mutual coupling, that is, that appearing between those nonresonant elements intended for the low frequency region (port 1 and port 3) with respect to the previous situation where the slots were not considered (Fig. 9).

As seen in the simulated results (Fig. 4), the slots attain similar impedance bandwidths at both frequency regions with the advantage of providing lower transmission coefficients. Namely, the slots introduce two significant dips in the low frequency region. These drops can be easily adjusted through the capacitors connected to the open edges of the slot. In this way, the capacitor of slot a produces a drop at 0.95 GHz whereas the capacitor at slot b produces a drop at 0.85 GHz (Fig. 10).

The antenna efficiency remains comparable to the case where the slots were not considered (Fig. 11). Moreover, the correlation values are significantly improved as two correlation dips appear at those frequencies where the slots are tuned. The solution attains correlation values below the threshold of 0.5 almost across the entire frequency range associated to the low frequency region (824–960 MHz) (Fig. 12). For the high frequency region (1710–2170 MHz), the correlation values are below 0.15 (Fig. 13).

The comparison between the radiation patterns measured at those ports intended for the low frequency region, namely port 1 and port 3, illustrates the differences that produce the correlation null found at a frequency close to 0.95 GHz (Fig. 14). In particular, the null found at port 1 when considering the prototype integrating the slots appears at a direction close to $\phi = 180°$, $\theta = 150°$. In contrast, this null appears at a direction close to $\phi = 100°$, $\theta = 40°$, when port 3 is measured, thus illustrating a rotation of the radiation pattern, which is the responsible of the correlation coefficient null close to these frequencies.

Finally, η_{MUX} is calculated for both prototypes using (2) with the measured envelope correlation and antenna efficiencies (Fig. 15). It is observed that the prototype including the slots improves the η_{MUX} in the low frequency region due to a better isolation that enhances correlation.

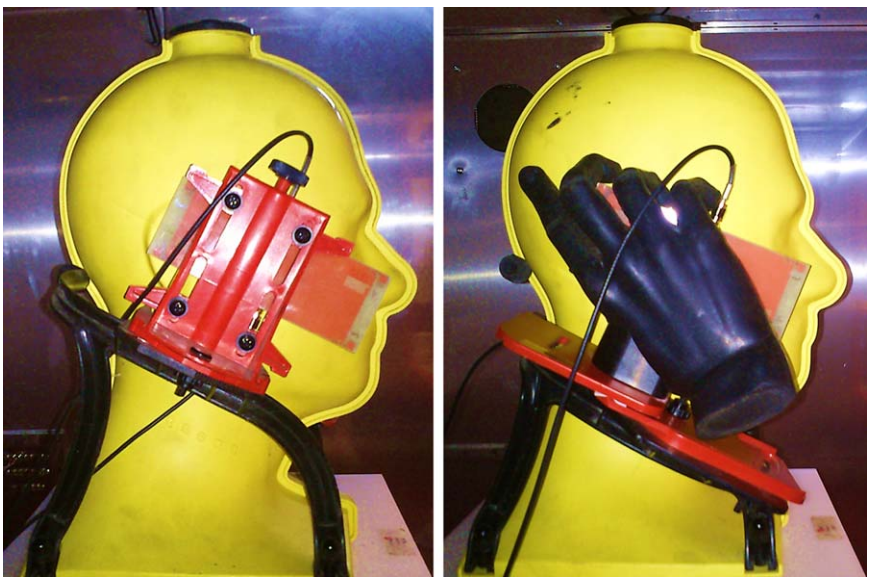

Figure 16 Set-up for capacity MIMO measurement taking into account a phantom head (left) and a phantom head including a phantom hand (right). Measurements are performed inside a reverberation chamber from Emite. [Color figure can be viewed in the online issue, which is available at wileyonlinelibrary.com]

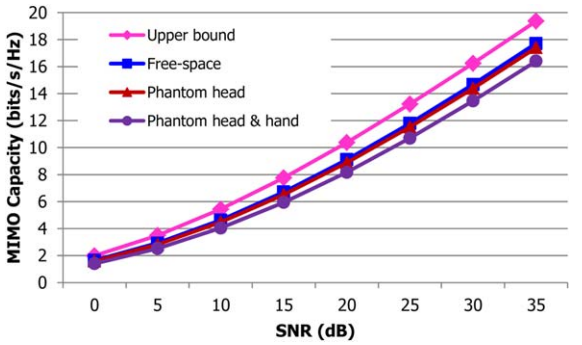

Figure 17 Measured MIMO capacity for 824–960 MHz in free-space, with a phantom head, and a phantom head with a phantom hand. [Color figure can be viewed in the online issue, which is available at wileyonlinelibrary.com]

5. MIMO CAPACITY MEASUREMENTS

The MIMO capacity for the prototype is measured in free-space, with a phantom-head and with a phantom-head including the effect of a phantom hand (Fig. 16). The MIMO capacity is measured in a reverberation chamber emulating a multipath environment having a Rayleigh statistics.

It is observed that for the free-space scenario, the measured capacity considering the Rayleigh environment is close to the ideal bound for a MIMO system of order 2 (Figs. 17, 18).

It is also interesting to analyze the impact on MIMO capacity as a function of both the head and hand. It is observed that capacity is more affected at the low frequency region, in particular when both the head and hand are considered while for the high-frequency region the capacity slight reduced when considering both the head and hand whereas the impact is minimum for the other cases.

6. CONCLUSION

A multiband MIMO antenna solution using small nonresonant elements of only $5 \times 5 \times 5$ mm^3 has been proposed. By integrating two miniaturized Hilbert slots, correlation values across the entire frequency range associated to the low frequency region has been significantly reduced. Not only the correlation values are below the threshold of 0.5 along the whole range but also two correlation nulls appear at those frequencies where the slots are tuned. Similarly, the transmission coefficient is minimized and two significant dips also appear at the frequencies where the slots are tuned. In the high frequency region, the correlation values remain below 0.1 across the entire frequency range and the antenna efficiency remain at high values. In addition, it provides the flexibility to tune the correlation and transmission coefficient nulls at the desired frequencies, since they can be easily adjusted through the series capacitor connected to the open edges of the Hilbert-based slots. Measured MIMO capacity shows values close to the ideal bound, thus, the proposal provides a 2×2 MIMO system capable of operating at several communication standards of 2G, 3G, and 4G. Accordingly, this solution positions as a good alternative to provide a compact multiband MIMO system capable of being integrated in current handset platforms.

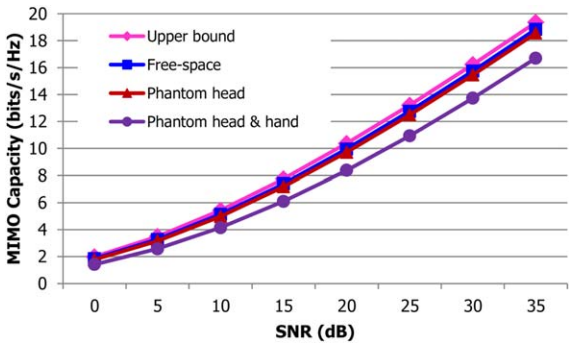

Figure 18 Measured MIMO capacity for 1710–2170 MHz in free-space, with a phantom head, and a phantom head with a phantom hand. [Color figure can be viewed in the online issue, which is available at wileyonlinelibrary.com]

ACKNOWLEDGMENT

The research project has been cofinanced by the Spanish Ministry of Industry, Energy, and Tourism belonging to the National Plan of Scientific Research, Development, and Technology Innovation. Project Ref: TSI-020100-2010-349.

REFERENCES

1. J.P. Arogyaswami, A.G. Dhananjay, U.N. Rohit, and B. Helmut, An overview of MIMO communications—A key to gigabit wireless, Proc IEEE 92 (2004), 198–218.
2. A.A.H. Azremi, M. Kyro, J. Ilvonen, J. Holopainen, S. Ranvier, C. Icheln, and P. Vainikainen, Five-element inverted-F antenna array for MIMO communications and radio-finding on mobile terminal. In: Loughborough Antennas and Propagation Conference, Loughborough, UK, November 2009, pp. 557–560.
3. Z. Li, Z. Du, and K. Gong, Compact reconfigurable antenna array for adaptive MIMO systems, IEEE Antennas Wireless Propag Lett 8 (2009), 1317–1320.
4. R. Glogowski and C. Peixeiro, Multiple printed antennas for integration into small multistandard handsets, IEEE Antennas Wireless Propag Lett 7 (2008), 632–635.
5. Y. Gao, X. Chen, Z. Ying, and C. Parini, Design and performance investigation of a dual-element PIFA array at 2.5 GHz for MIMO terminal, IEEE Trans Antennas Propag 55 (2007), 3433–3441.
6. M. Kyrö, M. Mustonen, C. Icheln, and P. Vainikainen, Dual-element antenna for DVB-H terminal. In: Loughborough Antennas and Propagation Conference, Loughborough, UK, March 2008, pp. 265–268.
7. S.K. Chaudhury, H.J. Chaloupka, and A. Ziroff, Novel MIMO antennas for mobile terminals. In: Proceedings of the 38th European Microwave Conference, Amsterdam, The Netherlands, October 2008, pp. 1751–1754.
8. P. Vainikainen, M. Mustonen, M. Kyrö, T. Laitinen, C. Icheln, and J. Villanen, Recent development of MIMO antennas and their evaluation for small mobile terminals. In: 17th International Conference on Microwaves, Radar and Wireless Communications, MIKON 2008, Wroclaw, May 2008, pp. 1–10.
9. S.K. Chaudhury, W.L. Schroeder, and H.J. Chaloupka, Multiple antenna concept based on characteristic modes of mobile phone chassis. In: Proceedings of the Second European Conference on Antennas and Propagation, EuCAP 2007, Edinburgh, United Kingdom.
10. Q. Rao and G. Wen, Ultra-small cubic folded strip antenna for handset devices. In: Proceedings of the IEEE Antennas and Propagation Society International Symposium, San Diego, CA, July 2008.
11. K.-L. Wong, C.-H. Chang, B. Chen, and S. Yang, Three-antenna MIMO system for WLAN operation in a PDA phone, Microwave Opt Technol Lett 48 (2006), 1238–1242.
12. D. Manteuffel, MIMO antenna design challenges. In: IEEE Antennas and Propagation Conference, Loughborough, UK, November 2009, pp. 50–56.
13. Q. Rao and D. Wang, A compact dual-port diversity antenna for long-term evolution handheld devices, IEEE Trans Vehicular Technol 59 (2010), 1319–1329.

14. S.B. Yeap, X. Chen, J.A. Dupuy, C.C. Chiau, and C.G. Parini, Integrated diversity antenna for laptop and PDA terminal in a MIMO system, IEE Proc Microwave Antennas Propag 152 (2005), 495–504.
15. S. Rowson, G. Poilasne, and L. Desclos, Isolated magnetic dipole antenna: application to GPS, Microwave Opt Technol Lett 41 (2004), 449–451.
16. M. Karaboikis, C. Soras, G. Tsachtsiris, and V. Makios, Compact dual-printed inverted-F antenna diversity systems for portable wireless devices, IEEE Antennas Wireless Propag Lett 3 (2004), 9–14.
17. J.-B. Yan, C.Y. Chiu, and R.D. Murch, Handset 4-port MIMO antenna using slit separated PIFA and quarter-wave slot antenna pair. In: Proceedings of the Antennas and Propagation Society International Symposium, San Diego, CA, 5–11 July 2008, pp. 1–4.
18. Y. Ding, Z. Du, and Z. Feng, A novel dual-band printed diversity antenna for mobile terminals, IEEE Trans Antennas Propag 55 (2007), 2088–2096.
19. A.S. Andrenko, T. Maniwa, and T. Yamagajo, Low correlation antenna design for diversity handset applications. In: IEEE Asia-Pacific Microwave Conference, APMC 2008, Macau, December 2008.
20. Q. Liu, Z. Du, K. Gong, and Z. Feng, A compact wideband planar diversity antenna for mobile handsets, Microwave Opt Technol Lett 50 (2008), 87–91.
21. Z. Li and Y. Rahmat-Samii, Optimization of PIFA-IFA combination in handset antenna designs, IEEE Trans Antennas Propag 53 (2005), 1770–1778.
22. C. Volmer, J. Weber, R. Stephan, K. Blau, and M.A. Hein, An eigen-analysis of compact antenna arrays and its application to port decoupling, IEEE Trans Antennas Propag 56 (2008), 360–370.
23. R.A. Bhatti, S. Yi, and S. Park, Compact antenna array with port decoupling for LTE-standardized mobile phones, IEEE Antennas Wireless Propag Lett 8 (2009), 1430–1433.
24. M. Shanawani, D.L. Paul, S. Dumanli, and C. Railton, Design of a novel antenna array for MIMO applications. In: 3rd International Conference on Information and Communication Technologies: From Theory to Applications, ICTTA 2008, Damascus, 2008.
25. S. Chang, Y.S. Wang, and S.J. Chung, A decoupling technique for increasing the port isolation between strongly coupled antennas, IEEE Trans Antennas Propag 56 (2008), 3650–3658.
26. B.K. Lau, J.B. Andersen, G. Kristensson, and A.F. Molisch, Impact of matching network on bandwidth of compact antenna arrays, IEEE Trans Antennas Propag 54 (2006), 3225–3228.
27. A. Diallo, C. Luxey, P. Le Thuc, R. Staraj, and G. Kossiavas, Study and reduction of the mutual coupling between two mobile phone PIFAs operating in the DCS1800 and UMTS bands, IEEE Trans Antennas Propag 54 (2006), 3063–3074.
28. A. Diallo, C. Luxey, P. Le Thuc, R. Staraj, and G. Kossiavas, Enhanced diversity antennas for UMTS handsets. In: Proceedings of the First European Conference on Antennas and Propagation, EuCAP 2006, Nice, France, November 2006.
29. G. Park, M. Kim, T. Yang, J. Byun, and A.S. Kim, The compact quad-band mobile handset antenna for the LTE700 MIMO application. In: Proceedings of the IEEE Antennas and Propagation Society International Symposium, Charleston, SC, June 2009.
30. K. Ishimiy, J. Langbacka, Z. Ying, and J. Takada, A compact MIMO DRA antenna. In: Proceeding of iWAT2008, Chiba, Japan, pp. 286–289.
31. S. Zhang, A.A. Glazunov, Z. Ying, and S. He, Reduction of the envelope correlation coefficient with improved total efficiency for mobile LTE MIMO antenna arrays: mutual scattering mode, IEEE Trans Antennas Propag 61 (2013), 3280–3291.
32. J. Anguera, A. Andújar, C. Puente, and J. Mumbru, Antennaless wireless device, Patent Application WO2010/015365, July 31, 2009.
33. J. Anguera, A. Andújar, C. Puente, and J. Mumbru, Antennaless wireless device capable of operation in multiple frequency regions, Patent Application WO2010/015364, July 31, 2009.
34. A. Andújar, J. Anguera, and C. Puente, Ground plane boosters as a compact antenna technology for wireless handheld devices, IEEE Trans Antennas Propag 59 (2011), 1668–1677.
35. A. Andújar, J. Anguera, C. Puente, and C. Picher, Wireless device capable of multiband MIMO operation, Patent Application WO 2012/017013, August 3, 2011.
36. A. Andújar and J. Anguera, MIMO multiband antenna system combining resonant and non-resonant elements, Microwave Opt Technol Lett 56 (2014), 1076–1084.
37. A. Andújar, J. Anguera, and Y. Cobo, Distributed systems robust to hand loading based on non-resonant elements, Microwave Opt Technol Lett 55 (2013), 2307–2317.
38. J. Anguera, C. Puente, E. Martínez, and E. Rozan, The fractal Hilbert monopole: a two-dimensional wire, Microwave Opt Technol Lett 36 (2003), 102–104.
39. C. Puente, E. Rozan, and J. Anguera, Space filling miniature antennas, Patent Application WO 01 54225, January 19, 2000.

MINIATURIZED RAT-RACE COUPLER WITH HARMONIC SUPPRESSION

Wei Nie,[1,2] Sha Luo,[2] Yongxin Guo,[2] and Yong Fan[1]
[1] EHF Key Laboratory of Fundamental Science, School of Electronic Engineering, University of Electronic Science and Technology of China, Chengdu 611731, Sichuan, People's Republic of China
[2] Department of Electrical and Computer Engineering, National University of Singapore, Singapore 117576, Singapore

Received 6 June 2014

ABSTRACT: *This article presents a miniaturized rat-race coupler with harmonic suppression. The proposed coupler only takes 15.1% of the area of the corresponding conventional rat-race coupler. By replacing the traditional transmission line with the proposed stub-loaded transmission line equivalently, the coupler performances can be retained and size can be reduced significantly at the same time. In addition, due to the transmission zero introduced by the stubs, the harmonic suppression is also improved. To verify the effectiveness of the substitution, the design equations are derived for analysis. Finally, the proposed coupler is fabricated for experimental verification, and a good match is found between the simulation and measurement results.* © 2015 Wiley Periodicals, Inc. Microwave Opt Technol Lett 57:190–193, 2015; View this article online at wileyonlinelibrary.com. DOI 10.1002/mop.28803

Key words: *rat-race coupler; miniaturization; harmonic suppression*

1. INTRODUCTION

A rat-race coupler is a critical component in microwave communication systems. Recently, a lot of miniaturization approaches have been used to reduce the size of a rat-race coupler, such as using shunt-stub-based artificial transmission lines [1], space filling curves [2], and implementing stepped-impedance transmission line sections [3]. In [4], $5\lambda/4$ and $7\lambda/6$ 3-dB couplers were proposed to reduce the circuit area. Meanwhile, attention has also been devoted to harmonic suppression of the rat-race coupler. In [5], compensated spiral compact microstrip resonant cell resonators were used to implement a compact rat-race coupler with harmonic suppression. In [6] and [7], size reduction and harmonic suppression were realized simultaneously using a defected ground structure and an electromagnetic bandgap element, respectively. In [8], the slow wave effects were produced by a shunt open stub and are used to miniaturize the occupying area and suppress higher order harmonics, respectively. But as the difficulty of slow effect accurate modeling still remains in [8], the design process is, therefore, complicated. The periodic stepped-impedance sections were used to achieve miniaturization and harmonic suppression in [9]. However, the mutual coupling among the stepped-impedance sections still needs optimization in simulation tool.

In this article, a new easy method to design miniaturized rat-race coupler with harmonic suppression is proposed by replacing